JOURNAL OF APPLIED ELECTROCHEMISTRY 19 (1989) 421–428

Electrochemical studies of lithium–boron alloys in non-aqueous media — comparison with pure lithium

P. SANCHEZ*, C. BELIN

Laboratoire des Agrégats Moléculaires et Matériaux Inorganiques, U.A. C.N.R.S. 79, U.S.T.L. — 2, place Eugène Bataillon, 34060 Montpellier Cédex, France

C. CREPY, A. DE GUIBERT

Laboratoires de Marcoussis, route de Nozay, 91460 Marcoussis, France

Received 17 July 1988; revised 25 November 1988

Lithium–boron alloy electrochemical properties were determined in some non-aqueous media by a.c. impedance and galvanostatic techniques and compared with pure lithium metal in terms of charge-transfer resistance and exchange current density. The behaviour of lithium–boron alloys with different compositions is correlated with the porosity of the refractory matrix by galvanostatic discharges and a.c. impedance measurements. Cycling tests were also reported for analysing the possibilities of replacing lithium metal by lithium–boron alloy.

1. Introduction

Pure lithium metal is now widely used as the negative electrode of high-energy advanced primary batteries [1, 2]. However, the possibility of anode melting at a relatively low temperature (180° C) easily leads to thermal runaway conditions in high power cell configurations.

Additional difficulties arise from the use of pure lithium in rechargeable cells. The major problems limiting cycle life are short circuits, caused by the growth of lithium dendrites through the separator, and poor cycling efficiency [3, 4]. These problems were partly solved by the use of the lithium–aluminium alloy [5, 6] but the two major drawbacks are: (i) loss of about 360 mV vs lithium metal potential; (ii) poor specific capacity ($\sim 0.79\,Ah\,g^{-1}$ at 25° C).

Lithium–boron alloy (70 w/o lithium) (LiB), first discovered by Wang [7], was found to be a good candidate as anode material in molten salt batteries [8–17]. This material can be described as metallic lithium contained in a solid porous matrix [18]. It has excellent chemical properties, a potential close to that of pure lithium and it remains solid at temperatures up to 600° C. Its good specific capacity ($\sim 1.92\,Ah\,g^{-1}$) makes it very attractive for use in non-aqueous batteries.

The purpose of this work was to study the electrochemical properties of the LiB alloys in non-aqueous media at room temperature. This material is compared with pure lithium in terms of exchange current density and charge-transfer resistance; galvanostatic discharges and cycling tests are also reported.

2. Experimental details

2.1. *Alloy preparation*

LiB alloy samples were prepared from lithium (Cogema, 99.94 pure) and crystalline boron (Johnson Matthey 99.5 w/o) using a procedure already described by Dallek [18]. In fact, such an alloy must be considered as a two-phase system consisting of metallic lithium contained in a porous refractory matrix. The matrix is an ionic compound with a stoichiometry close to $Li_{1.08}B$ [19]. Four LiB alloy samples with metallic lithium content ranging from 43 to 52 w/o (corresponding to alloy samples with total lithium content between 66.5 and 72 w/o) were prepared.

In a first approach, the extractable lithium amount was determined by differential scanning calorimetry (DSC) measurements [18]. These results were confirmed by ^{7}Li-nuclear magnetic resonance (NMR) alloy studies [19].

The alloy is less malleable than lithium metal, however it can easily be laminated into 0.1 mm thick sheets.

2.2. *Electrolytes*

The electrolyte used for this work was a solution of lithium hexafluoroarsenate ($LiAsF_6$ 1.5 M) (US Steel Agri Chemicals, electrochemical grade) in dioxolane (DOL). A.c. impedance measurements were also performed with a molar lithium perchlorate ($LiClO_4$) solution in propylene carbonate (PC). Cycling tests were carried out with both DOL–1.5 M $LiAsF_6$ and DOL–2 M $LiClO_4$.

* Author to whom correspondence should be addressed.

0021-891X/89 $03.00 + .12

2.3. *Cell preparation and test procedure*

The Teflon test cell was symmetrical with working and counter electrodes (10 mm in diameter, 0.4 mm thick) pressed onto stainless steel holders; the reference electrode was a Li metal lump. The cell was assembled and filled under dried argon in a glove box in order to protect the components from moisture, oxygen and nitrogen.

Cyclic voltammetry measurements were performed with an Edt ECP 133 potentiostat–galvanostat; the results were recorded on a TGM 164 Sefram plotter. The frequency response analysis was carried out with a Solartron mod. 1174 Schlumberger unit coupled with a potentiostat–galvanostat (Solartron mod. 1186); the results were recorded on an Apple II computer.

3. Results and discussion

3.1. *Exchange current density and polarization resistance of Li metal and LiB alloy in DOL–1.5 M $LiAsF_6$*

At low overpotentials, the reaction kinetics are independent of the interfacial ion concentration and controlled by the charge-transfer process. The exchange current densities and the polarization resistances were obtained by cyclic voltammetry as soon as the cell was

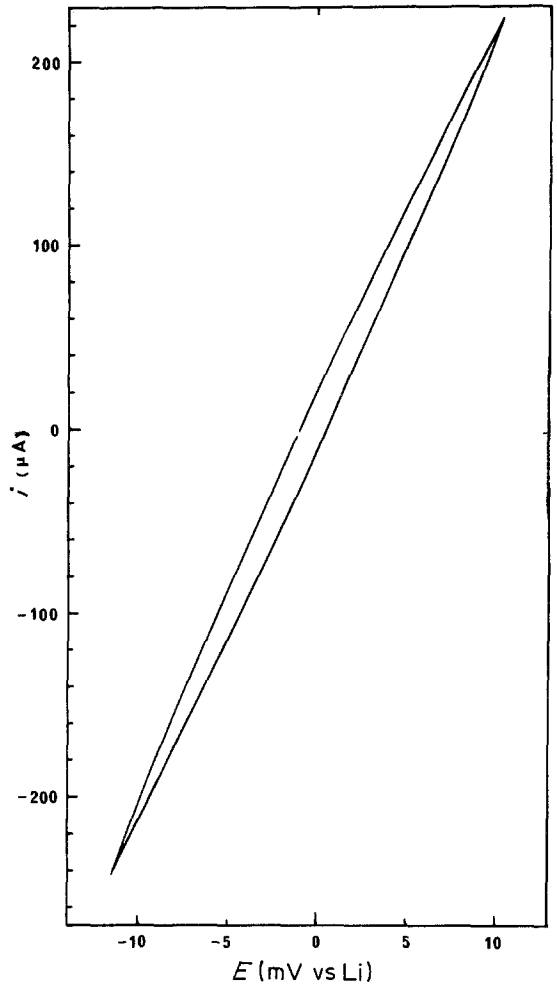

Fig. 1. Micropolarization curve of the Li electrode in DOL–1.5 M $LiAsF_6$ electrolyte (v = 1 mV s^{-1}, T = 25° C).

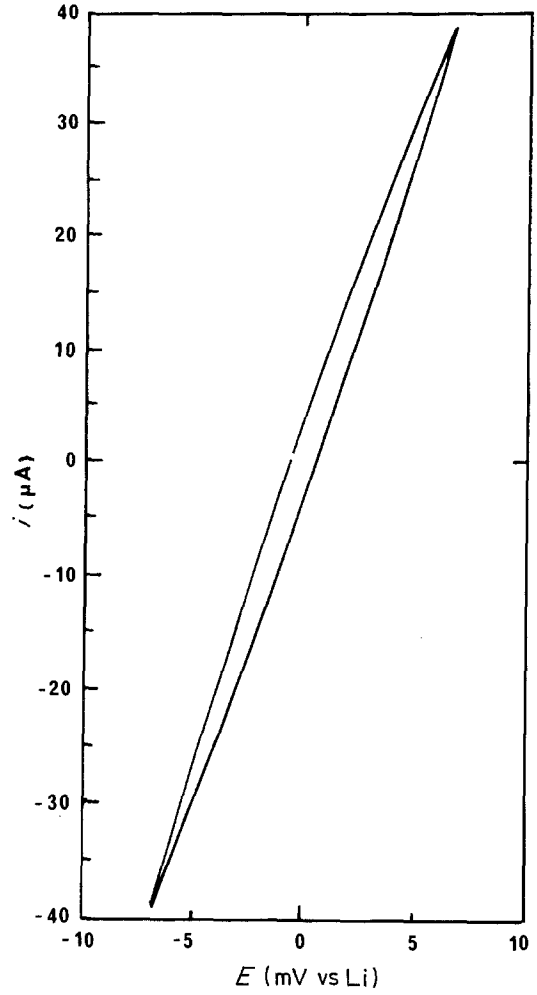

Fig. 2. Micropolarization curve of the LiB electrode in DOL–1.5 M $LiAsF_6$ electrolyte (v = 1 mV s^{-1}, T = 25° C).

assembled in order to limit spontaneous formation of a non-blocking passivation polymer film at the electrode surface [20, 21].

Assuming a single electron charge-transfer process, the polarization resistances were calculated from the slope of the linear micropolarization curves (Figs 1 and 2). The expression of the charge-transfer resistance related to the exchange current density is given, from the Butler–Volmer equation, by the relation [22]:

$$R_{pol} = (\delta\eta/\delta i)_{i=0} = \frac{RT}{F} \cdot \frac{1}{i_0}$$

where $R_{pol} = R_{film} + R_{ct}$ are respectively the resistance associated with the formation of the polymer film and the charge-transfer resistance; i_0 is the exchange current density; R, T and F have their usual meanings.

The polarization voltage, as shown on the micropolarization curves (Fig. 2), obtained by potentiometric

Table 1. Exchange current densities and polarization resistance for Li metal and LiB alloy (79 w/o) in DOL–0.5 M $LiAsF_6$

Electrode	i_0 (mA cm^{-2})	R_{pol} (Ω cm^2)
Li	0.2	124
LiB	0.7	37

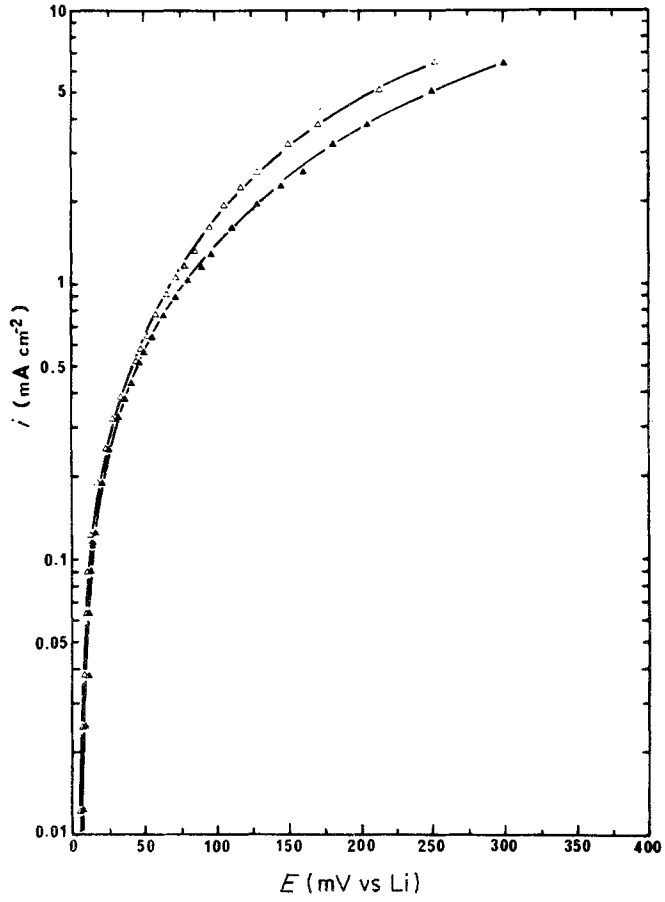

Fig. 3. Polarization curves of the Li (▲) and LiB (△) electrodes in DOL–1.5 M $LiAsF_6$ electrolyte at 25° C.

measurements is less significant for LiB than for Li metal.

The results obtained from the micropolarization curves are presented in Table 1.

LiB alloy (70 w/o) is a two-phase system containing a rigid porous matrix filled by metallic lithium. So, assuming that the electrochemical activity of lithium in LiB is very close to that of pure lithium metal, the ratio $R_{pol}(Li)/R_{pol}(LiB)$ near 3.5 implies that the LiB active surface is 3.5 times its geometrical surface. This result is in good agreement with the porous structure of the LiB matrix [18, 19]. The higher exchange current density obtained for LiB leads to a lower overpotential in the charge-transfer processes.

Polarization curves $I = f(E)$ (Fig. 3) were obtained in oxidation (dissolution of lithium) by potentiometric measurements.

Neither Li nor LiB exhibit a Tafel behaviour, implying a reaction, not only controlled by a charge-transfer process, but depending on a non-blocking passivation polymer film which readily forms as the cell is assembled; this layer is only partly destroyed under anodic polarization.

The kinetic parameters cannot be calculated from the Tafel plot, since the reaction is not purely charge-transfer controlled [22].

3.2. *A.c. impedance measurements*

A.c. impedance techniques are now widely used for interfacial electrochemical reaction studies. An electrochemical cell is, with respect to a low amplitude sinusoïdal perturbation, simply equivalent to an impedance. This impedance can be schematized by an electrical circuit (resistances and capacitances), represented in the Nyquist plan by a series of semicircles or arcs. Theoretically, each arc can be associated with a particular relaxation process (conduction, transfer, diffusion, etc.); identification of electrochemical processes can be achieved as soon as the electrochemical interface under investigation is sufficiently well known.

The experimental impedance diagrams of a lithium (or lithium alloy)/organic electrolyte interface generally show two or three semicircles, more or less centered on the real axis of the complex plane. Different theoretical models (solid electrolyte interface, porous polymer interface, binary electrolyte interface) have been proposed to take these results into account [24, 25]. Some features are common to all models, in particular the charge-transfer process taking place in the intermediate range frequencies: the equivalent circuit associated with this semicircle is the charge-transfer resistance (R_{ct}) in parallel with the double layer capacitance (C_{dl}). At low frequencies, except when a solid electrolyte is formed at the surface of lithium, a diffusion-controlled process is observed, with two different behaviours at very low frequencies, according to the thickness of the diffusion layer. For an infinite diffusion layer at a smooth electrode, the corresponding diagram is a straight line with a 45° slope (Warburg impedance); in the case of a finite thickness diffusion layer (e.g. diffusion through the film formed on lith-

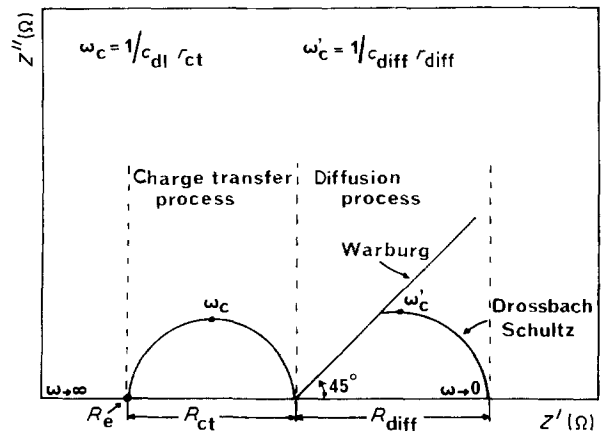

Fig. 4. Representation of a general impedance plot.

ium), an additional loop is observed at very low frequencies, according to the Drossbach–Schultz equation (Fig. 4) [26].

The third high-frequency semicircle, when present, can be associated with a conduction process through the passivation layer formed on the lithium surface.

Semicircles centered on the real axis are characteristic of smooth, flat electrodes. Centres of semicircles depressed from the real axis are observed in particular with rough or porous electrodes.

Our experimental measurements were performed for both pure lithium and LiB alloy electrodes in DOL–1.5 M $LiAsF_6$ and PC–1 M $LiClO_4$, first on freshly assembled cells. The experimental curves represented in the complex plane show the presence of two semicircles only. Characteristic resistances and capacitances were deduced from the experimental diagrams and are reported in Table 2.

For the dioxolane-based electrolyte, impedance data, as well as SEM examinations (not reported here), are compatible with the formation of a porous membrane on the lithium electrode. The high-frequency semicircle can be associated with the charge-transfer process, giving a double layer capacitance of a few μF, a common value for such a process. The double layer capacitance value for the LiB anode is more than twice the capacitance of the pure lithium electrode, corroborating the results deduced from the polarization measurements which suggested, with the alloy, the increase of the active surface. The low-frequency arc can be associated with the diffusion of Li^+ ions through the porous layer of finite thickness formed at the electrode/electrolyte interface.

The general shape of impedance diagrams (two semicircles) obtained with PC–$LiClO_4$ electrolyte and the pure lithium electrode is the same as that described by Warin [24], but the values of R_{ct}, C_{dl} and exchange current appear somewhat different. Our results are intermediate between those of Warin and Scrosati [26] who obtained a very low double layer capacitance. It would be beyond our scope to discuss in detail the origin of these differences; we only suggest that they stem from the different impurities present in the electrolytes, which alter the thickness and porosity of the passivating layer formed on the lithium surface. The noteworthy point is that the difference between pure lithium and LiB alloy remains the same as with the DOL–$LiAsF_6$ electrolyte. This shows that each anode/electrolyte interface maintains its own characteristics, depending on the nature of the electrolyte. In the two electrolytes experienced, the use of LiB alloy is equivalent to an increase of exchange current per cm^2 of geometrical surface of the electrode.

In order to take into account the growth of the passivation layer formed upon storage of electrodes in the electrolyte, the values of charge-transfer resistance and capacitance were measured after different periods of storage, in the DOL–$LiAsF_6$ electrolyte. Results are given in Table 3. Impedance spectra are depicted in Figs 5 and 6. As described by some authors [20, 21], we notice a growth of the passivating film with time of storage, in agreement with the increasing values of the charge-transfer resistance. Nevertheless, these values remain lower for the LiB sample.

For Li metal, the diffusion resistance varies from 16.5 to 60.6 Ωcm^2, while it remains constant for the LiB samples, results consistent with their porous structure which allows reaction of Li^+ ion at preferred sites.

3.3. *Galvanostatic discharges*

Galvanostatic discharges were performed at different current densities ranging from 0.5 to 100 mA cm^{-2}, in DOL–1.5 M $LiAsF_6$. Four LiB alloy compositions were studied; Li metal was also tested as reference. The discharge efficiency ($R = Li_{extracted}/Li_{extractable}$) was then plotted versus current density and is represented in Fig. 7.

The log/log plot exhibits three linear domains. At low current densities, the discharge efficiency is close to the theoretical ($R = 100\%$) for the different LiB compositions. At intermediate current densities, a smooth and linear decrease of R is observed with the

Table 2. Electrochemical parameters of Li and LiB (70 w/o) samples, deduced from impedance data

Electrode	*Electrolyte*	R_{ct} (Ωcm^2)	C_{dl} ($\mu F cm^{-2}$)	i_0 (mA cm^{-2})	R_{diff} (Ωcm^2)	C_{diff} (mF cm^{-2})
Li	DOL–1.5 M $LiAsF_6$	36.7	5.1	0.7	16.5	16.3
LiB	DOL–1.5 M $LiAsF_6$	7.8	11.9	3.3	10.9	74.4
Li	PC–1 M $LiClO_4$	90.0	1.1	0.28	58.7	4.5
LiB	PC–1 M $LiClO_4$	37.8	4.7	0.69	29.8	57.9
Li [24]	PC–1 M $LiClO_4$	5.0	6.0	3.3	5.0	
Li [26]	PC–1 M $LiClO_4$	120.0	0.03	0.2		

Table 3. Impedance data for Li and LiB (70 w/o) versus time of storage in DOL–1.5 M $LiAsF_6$

t	*Li*				*LiB*			
	R_{ct} (Ωcm^2)	C_{dl} ($\mu F cm^{-2}$)	R_{diff} (Ωcm^2)	C_{diff} ($mF cm^{-2}$)	R_{ct} (Ωcm^2)	C_{dl} ($\mu F cm^{-2}$)	R_{diff} (Ωcm^2)	C_{diff} ($mF cm^{-2}$)
0	36.6	5.1	16.5	16.3	7.8	11.9	10.9	74.4
6j	160.7	5.6	53.8	5.9	34.3	12.1	7.8	921.8
15d	171.6	4.9	60.6	5.9	42.9	10.0	7.0	773.1

same plot for the four samples. At high rates, there is a drastic decrease in efficiency; the decrease is higher for the samples with the lower lithium content. In comparison, the discharge efficiency of the lithium electrode taken as a reference exhibits only a small decrease while increasing the current density, due to shedding and loss of active material at high rates.

In the absence of other chemical reactions, such a linear dependence of efficiency on the discharge rate is usually characteristic of porous electrodes. Peukert [27] proposed the empirical formula $C = kI^{-n}$ between the discharged capacity C and the current density I for porous electrodes of lead–acid batteries (k is a constant, depending on the temperature and features of the experimental cell). This formula is valid in the low to medium current density domain, where the discharge kinetics are charge-transfer limited, the coefficient n of the formula being only related to the geometry of the porous electrode. Le Méhauté *et al.* recently established a generalization of Peukert's law considering the battery electrodes as fractal objects [28]. This generalization gives a theoretical basis to the empirical Peukert formula, and allows explanation of the linear behaviour of the log/log plot at high rates, which corresponds to diffusion-limited kinetics in the porous electrode. The exponent n of the law $C = kI^{-n}$ is then related to the fractal dimension of the porous material.

In summary, the three linear domains of the log/log plot all correspond to a discharge law $C = kI^{-n}$, and can be described as follows:

(i) A Faradic domain ($n = 0$) at low current density where the theoretical capacity of the system can be restored.

(ii) A transfer domain ($0 < n < 1$) where the capacity decreases slowly with the applied current density; the kinetic reaction is then controlled by a charge-transfer process.

(iii) A diffusion domain ($n > 1$) showing a drastic discharge efficiency drop at high current density.

The differences in high-rate slopes in Fig. 7 for the different LiB samples are very interesting, since they give indirect information about the various porosities of the matrix in the samples. A lower slope (higher discharge efficiency) would correspond to a more open porosity of the matrix, allowing a better accessibility

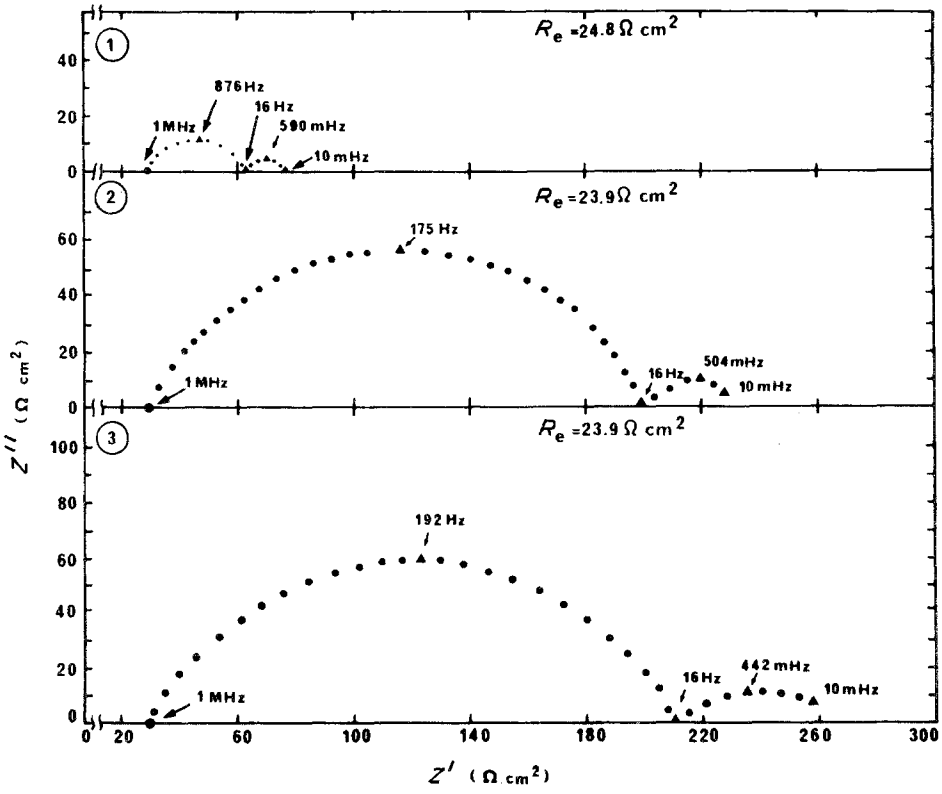

Fig. 5. Impedance plot of the Li electrode in DOL–1.5 M $LiAsF_6$ electrolyte at different times of storage at 25°C. Frequency range: 10 mHz–1 MHz. (1) After assembling the cell; (2) after 6 days of storage; (3) after 15 days of storage.

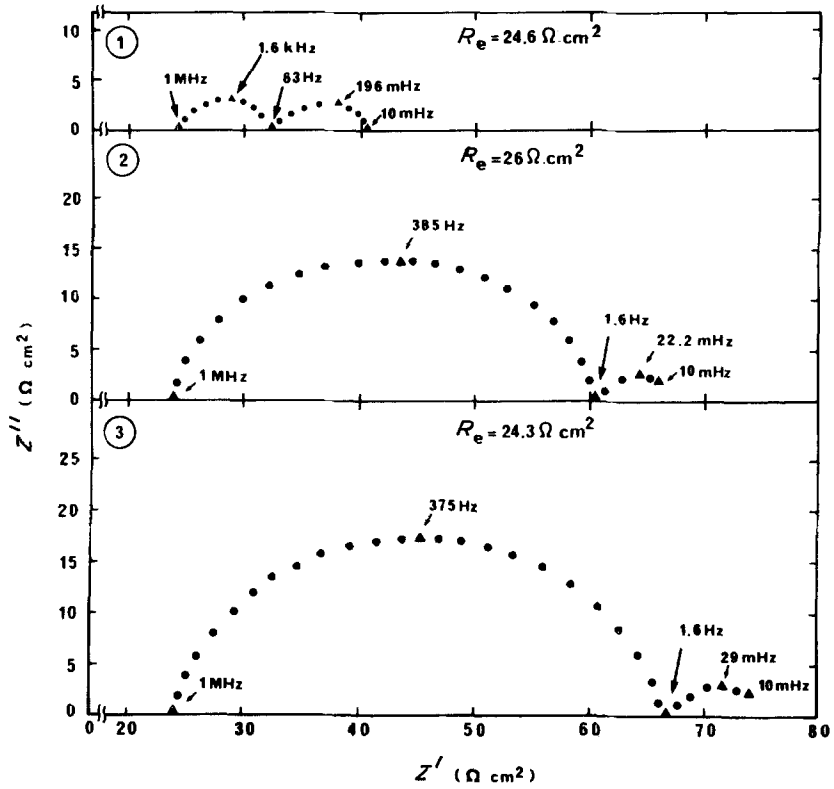

Fig. 6. Impedance plot of the LiB electrode in DOL–1.5 M $LiAsF_6$ electrolyte at different times of storage at 25° C. Frequency range: 10 mHz–1 MHz. (1) After assembling the cell; (2) after 6 days of storage; (3) after 15 days of storage.

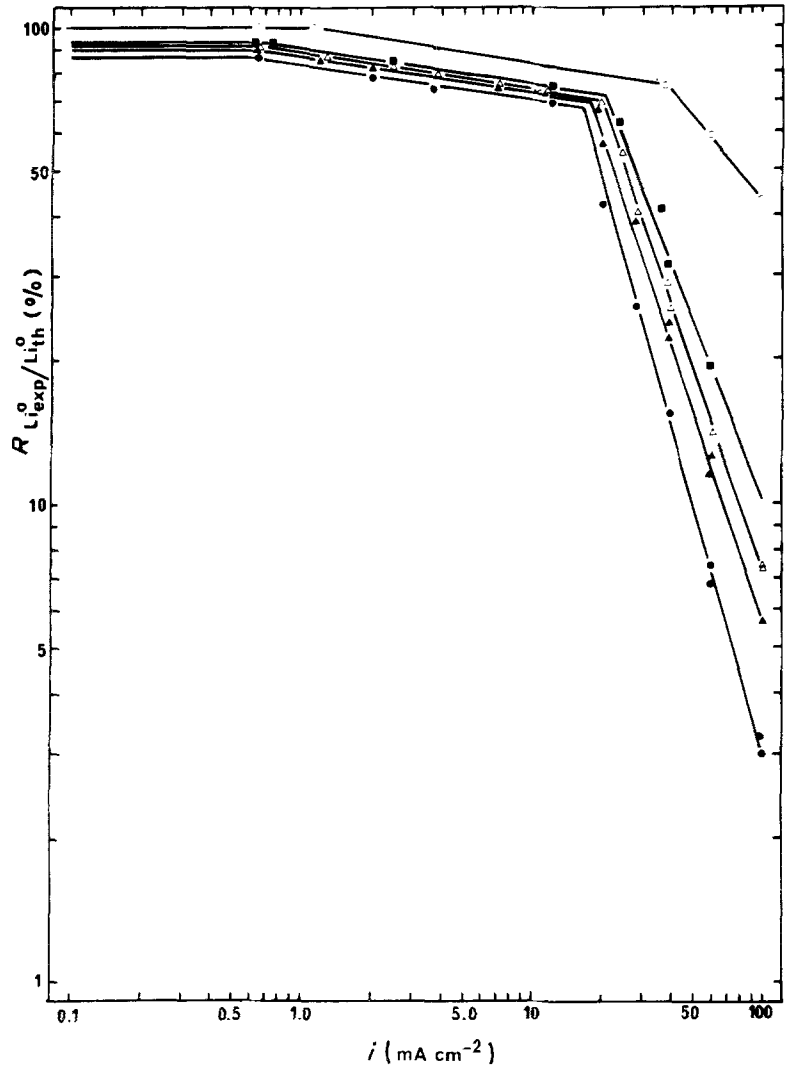

Fig. 7. Peukert's law for Li (○) and different LiB alloy compositions (metallic lithium content: 43% (●), 45% (▲), 50% (△), 52% (■)) in DOL–1.5 M $LiAsF_6$ electrolyte at 25° C.

Table 4. Cycling tests results

Electrolyte	*Overpotential* (mV)	*d.o.d.* (%)	*i* ($mA\,cm^{-2}$)	*Cycles*
DOL–2 M $LiClO_4$	200	25	0.5	6
DOL–1.5 M $LiAsF_6$	80	20	1.0	20
DOL–1.5 M $LiAsF_6$	240	40	5.0	4

and an easier diffusion of lithium through the pores. This more open porosity is obtained with the higher lithium content.

These results were confirmed by the analysis of the porous matrix after discharge. The porous matrices are extremely reactive and cannot be analysed by usual techniques such as BET area measurements. In a first approach, two LiB matrix samples (43 w/o and 52 w/o metallic lithium content) were characterized by a.c. impedance measurements after complete extraction. Measurements of the double layer capacitances (C_{dl}) allowed us to reach the developed surfaces; they were found close to $0.18\,m^2g^{-1}$ and $0.41\,m^2g^{-1}$ for the LiB 43 w/o and 52 w/o metallic lithium content, respectively. These results are in full agreement with the high rate discharge behaviour. They show that efficiency is not only related to the metallic lithium content, but also to the matrix porosity. Further studies are in progress to develop these results [19].

3.4. *Cycling tests*

As discussed at the beginning of this paper, the behaviour of electrochemical cells during cycling is often limited by negative electrode problems (dendritic growth of lithium, short-circuiting, etc.). The use of lithium alloys such as LiAl or LiSi has been suggested in order to overcome these difficulties. However, the use of these two alloys leads to a voltage loss of the cells, which is detrimental to the overall energy density of the battery. The advantageous properties of LiB alloy in terms of voltage discharge make it very attractive for use in non-aqueous batteries. Cycling tests were performed to analyse the behaviour of LiB alloy in some non-aqueous media during the charge–discharge process. The results are summarized in Table 4 (d.o.d.: depth of discharge).

The cycling results obtained in the case of LiB alloy do not compare favourably with those obtained for pure lithium or for lithium–aluminium alloy where a cycling efficiency of at least 97% is obtained in the same conditions [29]. The same problems as those already encountered for pure lithium were observed, but much earlier. A limited cycle number is observed (Fig. 8). Under more stringent conditions, the reversibility of the system decreased rapidly and only a few cycles were observed. The high voltage plateau which appears on discharged curves (Fig. 9) after a few cycles corresponds to the matrix discharge. During the charge process the discharged lithium cannot reach the inner cavities of the porous matrix and is electrodeposited at the surface with an efficiency lower than 100%; the consequence is a shift in the cycling domain during the following cycles. Finally the lithium chemically bound to boron also discharges completely and leads to the destruction of the matrix.

The number of cycles is too low for practical use in batteries operating at room temperature compared with the possibility of 1500 cycles for an aluminium substrate [6].

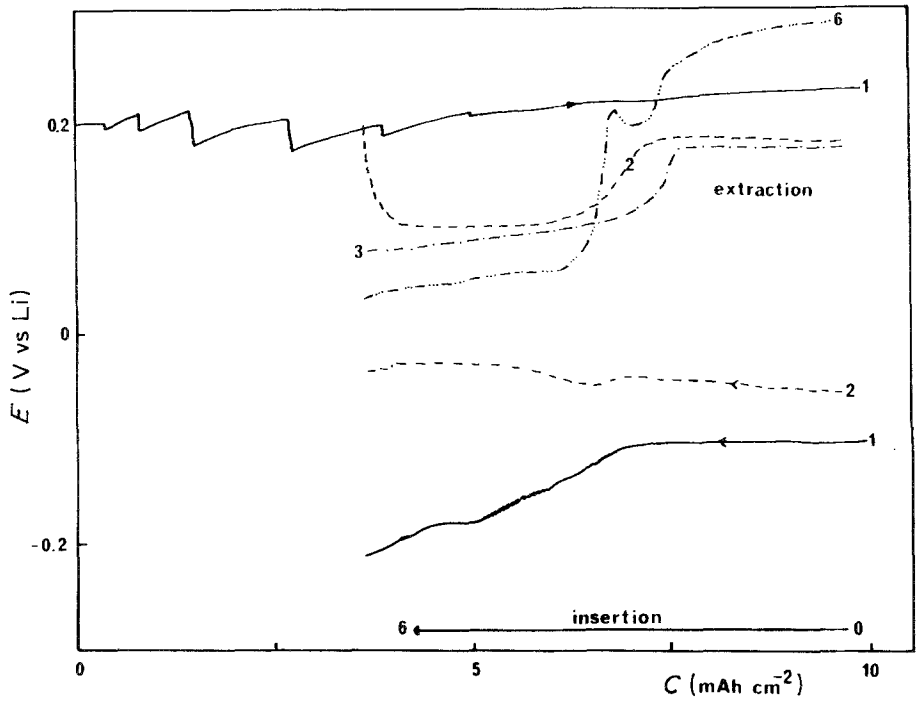

Fig. 8. Cycling test of LiB electrode in DOL–2 M $LiClO_4$ electrolyte at $i = 0.5\,mA\,cm^{-2}$ (25° C). Theoretical capacity of the electrode: 39 mAh. First extraction: 10 mAh, cycling depth: 6 mAh.

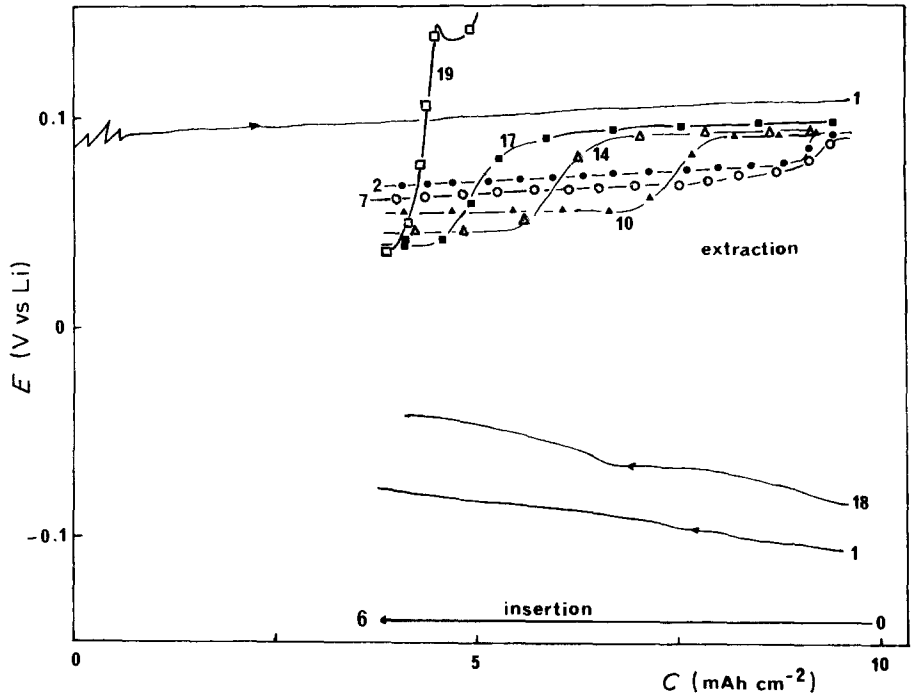

Fig. 9. Cycling test of LiB electrode in DOL–1.5 M $LiAsF_6$ electrolyte at $i = 1\,mA\,cm^{-2}$ (25° C). Theoretical capacity of the electrode: 44 mAh. First extraction: 10 mAh, cycling depth: 6 mAh.

4. Conclusion

The electrochemical parameters of LiB alloys were determined in some non-aqueous media; the importance of the metallic lithium content in the matrix was demonstrated and correlated to the matrix porosity. From the practical point of view, the results could be summarized as follows:

(i) Up to $10\,mA\,cm^{-2}$ at room temperature, LiB discharge efficiencies were found to be close to those for pure lithium metal, so this alloy can be used in systems where thermal runaway leads to cell destruction.

(ii) At high rates, discharge limitations arose from the porosity of the LiB matrix.

(iii) Although cycling possibilities greatly depend on the media used, LiB alloys present no better performance on cycling than Li metal.

Acknowledgements

This work was supported by the D.R.E.T. and one of us wishes to thank the C.N.R.S. for his grant.

References

[1] E. Yeager, Proceedings of the Workshop on Lithium Non-aqueous Battery Electrochemistry, Vol. 80–7, June 4–6 (1980) pp. 1–12.
[2] J. O. Besenhard and G. Eichinger, *J. Electroanal. Chem.* **68** (1976) 1.
[3] D. Linden, *J. Power Sources* **11** (1984) 87.
[4] B. Scrosati, *J. Power Sources* **11** (1984) 129.
[5] A. S. Baranski and W. R. Fawcett, *J. Electrochem. Soc.* **129** (1982), 901.
[6] I. Epelboin, M. Froment, M. Garreau, J. Thevenin and D. Warin, *J. Electrochem. Soc.* **127** (1980) 2100.
[7] F. E. Wang, US Patent Application No. 4, 110, 111 (1978).
[8] S. D. James and L. E. DeVries, *J. Electrochem. Soc.* **123** (1976) 321.
[9] L. E. DeVries, L. D. Jackson and S. D. James, *J. Electrochem. Soc.* **126** (1979) 933.
[10] S. Dallek, B. F. Larrick and R. Szwarc, Proceedings of 30th Power Sources Symposium, 7–12 June (1982) pp. 42–44.
[11] R. Szwarc, R. D. Walton, S. Dallek and B. F. Larrick, *J. Electrochem. Soc.* **129** (1982) 1168.
[12] B. F. Larrick, S. D. James and R. Szwarc, Proceedings of the 28th Power Sources Symposium (1978) pp. 95–98.
[13] R. Szwarc, R. D. Walton, NSWC/GEPP-TIS-451, Naval Surface Weapons Center, Silver Spring, MD, March 31 (1980).
[14] S. D. James, NSWC/TR-81-155, Naval surface Weapons Center, Silver Spring, MD, April (1981).
[15] S. D. James, *J. Appl. Electrochem.* **12** (1982) 317.
[16] R. Szwarc and S. Dallek, NSWC/GEPP-TM-645, Naval Surface Weapons Center, Silver Spring, MD, May (1982).
[17] P. Sanchez, C. Belin, J. P. Buchel and G. Crepy, to be published.
[18] S. Dallek, D. W. Ernst and B. F. Larrick, *J. Electrochem. Soc.* **126** (1979) 866.
[19] P. Sanchez and C. Belin, *C. R. Acad. Sci.*, Paris, 307(II) (1988), 2027.
[20] E. Peled, *J. Power Sources* **9** (1983) 253.
[21] A. N. Dey, *Thin Solids Films* **43** (1977) 131.
[22] A. J. Bard and L. R. Faulkner, 'Electrochimie', Masson, Paris (1983).
[23] E. J. L. Shouler, in 'Solid State Protonic Conductors III' (edited by J. B. Goodenough, J. Jensen and A. Potier), Odense University Press (Denmark) (1985) pp. 16–60.
[24] D. Warin, Thesis, Paris (1980).
[25] C. Dubois, Thesis, Paris VI (1987).
[26] S. Morzilli, F. Bonino and B. Scrosati, *Electrochim. Acta* **32** (1987) 961.
[27] W. Peukert, *Elektrotechn. Z.* **18** (1897) 287.
[28] L. Fruchter, G. Crepy and A. Le Mehaute, *J. Power Sources* **18** (1986) 51.
[29] A. de Guibert and A. Hermelin, unpublished results.